Research Square

Preprints are preliminary reports that have not undergone peer review.
They should not be considered conclusive, used to inform clinical practice,
or referenced by the media as validated information.

Cell-to-cell transmission of stress granules propagates integrated stress response

Tao Li

tli@ncba.ac.cn

Nanhu Laboratory, National Center of Biomedical Analysis https://orcid.org/0000-0002-0746-8322

Ming Zhao

Nanhu Laboratory, National Center of Biomedical Analysis https://orcid.org/0000-0002-7401-9332

Liu-Bing Yu

School of Basic Medical Sciences, Fudan University

Chen-Xin Liu

Institute of Translational Medicine, Zhejiang University https://orcid.org/0009-0009-6776-2281

Min-Yi Feng

Nanhu Laboratory, National Center of Biomedical Analysis

Xue-Qing Zhou

Nanhu Laboratory, National Center of Biomedical Analysis

Hui-Zi Yue

Nanhu Laboratory, National Center of Biomedical Analysis

Hong Cai

Nanhu Laboratory, National Center of Biomedical Analysis

Tian Xia

National Center of Biomedical Analysis https://orcid.org/0000-0002-1527-2194

Yu Yu

Nanhu Laboratory, National Center of Biomedical Analysis https://orcid.org/0000-0003-3708-508X

QiuYing Han

Nanhu Laboratory, National Center of Biomedical Analysis

Kai Wang

National Center of Biomedical Analysis

Xin Xu

Nanhu Laboratory, National Center of Biomedical Analysis

Li-Bing Yin

Nanhu Laboratory, National Center of Biomedical Analysis

Shou-Nian Li

Nanhu Laboratory, National Center of Biomedical Analysis

Liang Chen

National Center of Biomedical Analysis

Kun He

AiLing Li

Nanhu Laboratory, National Center of Biomedical Analysis

Xue-Min Zhang

National Center of Biomedical Analysis https://orcid.org/0000-0003-0207-4532

Tao Zhou

Nanhu Laboratory, National Center of Biomedical Analysis https://orcid.org/0000-0001-6222-2053

Wen Xue

Institute of Basic Medical Sciences, National Center of Biomedical Analysis

---

Biological Sciences - Article

Keywords:

Posted Date: June 2nd, 2026

DOI: https://doi.org/10.21203/rs.3.rs-9629444/v1

License: This work is licensed under a Creative Commons Attribution 4.0 International License.
Read Full License

Additional Declarations: There is **NO** Competing Interest.

Cell-to-cell transmission of stress granules propagates integrated stress response

Authors:

Ming Zhao[1,4], Liu-Bing Yu[1,2,4], Chen-Xin Liu[3,4], Min-Yi Feng[1], Xue-Qing Zhou[1], Hui-Zi Yue[1], Hong Cai[1], Tian Xia[1], Yu Yu[1], Qiu-Ying Han[1], Kai Wang[1], Xu Xin[1], Li-Bing Yin[1], Shou-Nian Li[1], Liang Chen[1], Kun He[1], Ai-Ling Li[1], Xue-Min Zhang[1], Tao Zhou[1,2,*], Wen Xue[1,*], Tao Li [1,2,3,*]

Affiliations:

[1] Nanhu Laboratory, State Key Laboratory of Biomedical Analysis (SKLBA, formerly known as National Center of Biomedical Analysis, NCBA), Beijing 100039, China.

[2] Key Laboratory of Medical Molecular Virology (MOE/NHC/CAMS), Shanghai Institute of Infectious Disease and Biosecurity, Shanghai Frontiers Science Center of Pathogenic Microorganisms and Infection, School of Basic Medical Sciences, Shanghai Medical College, Fudan University, Shanghai 200032, China.

[3] Institute of Translational Medicine, Zhejiang University School of Medicine, Hangzhou, Zhejiang 310029, China.

[4] These authors contributed equally to this work.

*Correspondence: tli@ncba.ac.cn; wxue@xmail.ncba.ac.cn; tzhou@ncba.ac.cn.

Abstract

The integrated stress response (ISR) is a conserved signaling network that enables cells to adapt to environmental stresses, and its dysregulation is implicated in numerous human diseases[1]. Although ISR activation is a cell-autonomous event, pathological tissues frequently display coordinated ISR activation across many cells. Whether local ISR activation spreads beyond the initially affected cells, and whether such spread contributes to pathology, remain poorly understood. Here, we identify the intercellular transmission of stress granules (SGs), a process we term Cell-to-cell Transmission of SGs (CTS), as the pivotal mechanism for ISR propagation. We show that, once formed, the SGs are released *via* TMED10-dependent unconventional secretion pathway and internalized by neighboring cells through

macropinocytosis. This CTS event is sufficient to instigate ISR in recipient cells in a PERK- and GCN2-dependent manner, thereby broadcasting the stress state across cell populations. Ablation of *G3BP1* in donor cells to prevent SGs formation, or inhibition of their secretion with 3-Methyladenine, potently suppressed ISR propagation. Consistently, disruption of macropinocytosis blocked SG uptake in recipient cells and consequently inhibited ISR. Crucially, in a murine model of renal ischemia-reperfusion injury, targeting either SGs formation, secretion, or uptake significantly mitigated tissue damage. These findings provide a mechanistic explanation for how the ISR expands from a cellular to a tissue scale and establish CTS as a therapeutically tangible target for mitigating ISR-associated pathologies.

Main Text

The integrated stress response (ISR) is a conserved signaling network that enables eukaryotic cells to sense diverse environmental and physiological challenges and mount adaptive transcriptional and translational programs[1,2]. Transient ISR activation restores homeostasis, but sustained or dysregulated signaling drives detrimental effects, cell death, and pathogenesis of numerous conditions, including neurodegeneration, metabolic disease, and ischemia-reperfusion injury[1,3]. Under *in vivo* conditions, injury often begins in spatially restricted subsets of cells yet progresses into broader tissue dysfunction[4]. How a stress response initiated locally becomes amplified into coordinated, tissue-scale pathology remains obscure. Resolving this gap would connect cell-autonomous stress adaptation to multicellular disease progression and may reveal new opportunities for therapeutic intervention.

A central event in ISR activation is phosphorylation of the eukaryotic translation initiation factor 2α (eIF2α) by stress-sensing kinases, which suppresses bulk translation while allowing selective translation of adaptive mRNAs such as activating transcription factor 4 (ATF4)[2,5]. Stress granules (SGs) are dynamic cytoplasmic condensates that assemble rapidly during ISR activation[6-8]. They contain untranslated mRNAs together with scaffold and RNA-binding proteins such as ras GTPase-activating protein-binding protein (G3BP) and cytotoxic granule associated RNA binding protein (TIA-1) and are widely regarded as hallmarks of translational arrest[7,9]. Yet, it is reported that global translation repression can occur independently of SG

assembly[10-12], indicating that SG formation serves a function distinct from the initial translational block. This, together with the selective partitioning of specific mRNAs and regulatory proteins into SGs[7,13,14], suggests that SGs may actively modulate stress adaptation, potentially serving as enriched carriers of signaling molecules. Concurrently, intercellular transmission of stress has been observed in several physiological and pathological settings[4,15], but the responsible molecular vehicles remain unclear. These observations raise the possibility that SGs themselves might function as transmissible effectors that broadcast stress to neighboring cells.

Intercellular communication occurs through classical, signal peptide-dependent secretion *via* the ER-Golgi pathway, as well as through unconventional protein secretion (UPS) of cytosolic, leaderless proteins (Types I–IV)[16,17]. Additionally, extracellular materials can be internalized by recipient cells through various uptake pathways, including macropinocytosis[18,19]. These pathways provide plausible routes for SG transfer, but whether SGs are actively secreted, taken up by recipient cells and functionally capable of triggering ISR signaling has not been demonstrated. In the current study, we identify cell-to-cell transmission of stress granules (CTS) as a mechanism that propagates ISR activation across cell populations, providing a conceptual framework for how local ISR activation may scale to tissue-level pathology, and highlighting SG transmission as a therapeutically actionable axis in ISR-associated diseases.

Results

Stress granules undergo cell-to-cell transmission

To test the hypothesis that SGs act as transmissible effectors of stress, we first investigated whether they can move between cells. Because SGs are induced broadly by ISR-activating stimuli[6,7], we confirmed robust SG assembly in multiple human cell types, including the cardiomyocyte cell line AC16, and the renal tubular epithelial cell line HK-2, following treatment with sodium arsenite or poly(I:C) (Extended Data Fig. 1a–d). We next sought to visualize intercellular SG transfer directly. To do this, we established an optogenetic SG

system (Opto-SGs) by fusing the light-sensitive protein Cryptochrome 2 (Cry2) and the fluorescent protein mCherry to the SG scaffold protein G3BP1, enabling spatiotemporal control of SG assembly in AC16 cells. We then co-incubated Opto-SGs cells with control AC16 cells that express G3BP1-mEGFP (Extended Data Fig. 2a). Upon blue-light stimulation, we observed the time-dependent appearance of Cry2-mCherry-G3BP1 condensates in the Opto-SG-carrying cells (Fig. 1a and Supplementary Video 1). Strikingly, these mCherry-positive puncta subsequently became detectable inside the G3BP1-mEGFP-expressing cells (Fig. 1a), suggesting that SGs can transfer from donor to recipient cells.

To verify this observation, we generated HK-2 cell lines stably expressing either mCherry-G3BP1 or G3BP1-mEGFP (Extended Data Fig. 2b). Sodium arsenite and poly(I:C) robustly induced cytoplasmic SG formation in both lines (Extended Data Fig. 2c). When the two types of cells were co-cultured and challenged, we detected bidirectional transfer of SG puncta, as evidenced by mEGFP-positive puncta (green) in mCherry-G3BP1-expressing (magenta) cells, and mCherry-positive puncta in G3BP1-mEGFP-expressing cells (Fig. 1b).

To determine whether CTS requires direct cell-cell contact, we employed a Transwell co-culture system. Unlabeled recipient HK-2 cells were seeded in the lower chamber. Stress challenged donor cells, HK-2-expressing mCherry-G3BP1, were placed in the upper chamber. We found that mCherry-positive SG puncta became detectable in recipient cells in the lower chamber (Fig. 1c), indicating that CTS can occur without direct cell-cell contact. To directly examine whether SG-like condensates can be taken up by recipient cells, we purified recombinant mEGFP-G3BP1 (Extended Data Fig. 2d) and incubated it with poly(A) to induce droplet formation *in vitro* (Extended Data Fig. 2e and Supplementary Video 2). When these pre-assembled droplets were added to HK-2 cells, they were readily internalized by these cells (Fig. 1d and Extended Data Fig. 2f,g and Supplementary Video 3). Together, these data show that SGs can be released from donor cells and be internalized by recipient cells independently of direct cell-cell contact. We thus refer to this process as cell-to-cell transmission of stress granules (CTS).

CTS mediates propagation of the ISR

We next investigated the function of CTS. The cells following uptake of mEGFP-G3BP1:poly(A) droplets were subjected to RNA sequencing, which revealed the enrichment of stress-response pathways by gene ontology (GO) analysis (Fig. 1e), including ISR-related pathways, which suggested that CTS elicits an ISR-like program in recipient cells.

To determine whether this response specifically depends on the transmission of SGs, we generated *G3BP1*-deficient HK-2 cells and a matched rescue line (Extended Data Fig. 3a). Consistent with previous studies[11,12,14,20-23], loss of G3BP1 abolished SG formation (Extended Data Fig. 3b), but did not significantly impair cell-autonomous ISR activation, as assessed by puromycin incorporation, eIF2α phosphorylation, and the induction of ISR downstream effectors ATF4, GADD34 and CHOP (Extended Data Fig. 3c,d). Thus, SGs are dispensable for cell-autonomous ISR activation. Using the Transwell system, we found that poly(I:C) or arsenite treatment to donor cells in the upper chamber elicited a canonical ISR in recipient cells in the lower chamber, characterized by reduced global protein synthesis, increased eIF2α phosphorylation, and induction of ATF4, GADD34 and CHOP (Fig. 1f–j). In contrast, when *G3BP1*-deficient cells were used as donors, the ISR activation in recipient cells was abolished (Fig. 1f–j). Re-expression of *G3BP1* in donor cells restored ISR activation in recipients (Fig. 1f–j). With reconstituted G3BP1 condensates, we further demonstrated that the engulfment of SG-like droplets induced ISR activation in recipient cells (Fig. 1k,l).

To distinguish whether ISR propagation requires G3BP1 in its soluble or condensed form, we fused a cell-penetrating TAT peptide to mEGFP-G3BP1 (Extended Data Fig. 3e), enabling direct delivery of soluble G3BP1 into cells (Extended Data Fig. 3f). Notably, TAT-mEGFP-G3BP1 failed to induce ISR activation (Extended Data Fig. 3g,h), indicating that the condensed, rather than soluble, form of G3BP1 is required to transmit stress signaling. Collectively, these results show that CTS is a critical mechanism for propagating ISR activation across cells.

PERK and GCN2 are important for CTS-induced ISR activation

Phosphorylation of eIF2α is a defining feature of the ISR and is mediated by either one of the four stress-sensing kinases, eukaryotic translation initiation factor 2 alpha kinase 1

(EIF2AK1), EIF2AK2, EIF2AK3 and EIF2AK4, also known as HRI, PKR, PERK and GCN2[1,2]. To identify which kinase mediates ISR activation following condensate uptake, we individually knocked down each kinase in HK-2 cells (Fig. 2a) and treated the cells with mEGFP-G3BP1:poly(A) droplets. Our data showed that the depletion of either *PERK* or *GCN2* markedly attenuated CTS-induced ISR activation, whereas knockdown of *PKR* or *HRI* had no significant effect (Fig. 2b,c).

We next generated *GCN2*- and *PERK*-deficient HK-2 cells along with corresponding rescue lines. Because poly(I:C) and arsenite primarily signal through PKR and HRI[24,25], respectively, the deficiency of GCN2 or PERK did not impair cell-autonomous ISR activation following these stimuli (Fig. 2d,e and Extended Data Fig. 4a,b). By contrast, loss of GCN2 or PERK abolished ISR activation induced by mEGFP-G3BP1:poly(A) droplets, and re-expression of the corresponding kinase restored this response (Fig. 2f,g and Extended Data Fig. 4c,d). We then examined whether these kinases in recipient cells are required for intercellular ISR propagation. Using wild-type HK-2 cells as donors in the upper chamber and *GCN2*-deficient cells as recipients in the lower chamber, stress induction in donor cells triggered ISR activation in wild-type recipients but not in GCN2-deficient recipients (Fig. 2h–l). Similar results were obtained using PERK-deficient recipient cells (Extended Data Fig. 4e–i). Thus, GCN2 and PERK in recipient cells are essential for the initiation of ISR triggered by CTS.

To investigate how CTS engages these kinases, we examined whether GCN2 and PERK are associated with internalized SG-like condensates. Following incubation with mEGFP-G3BP1:poly(A) droplets, both GCN2 and PERK localized into the internalized condensates (Fig. 2m and Extended Data Fig. 4j). This spatial association suggests that internalized SG-like assemblies may recruit and facilitate the activation of GCN2 and PERK, thereby transducing signals from CTS to ISR activation.

TMED10-dependent type III UPS mediates SG release for ISR propagation

Having established that CTS is required for intercellular ISR propagation, we then turned to study the mechanism of SG release from donor cells. Following arsenite or poly(I:C)

stimulation, core SG components, including G3BP1 and TIA-1, were detected in the culture medium (Extended Data Fig. 5a,b), indicating the extracellular release. Moreover, co-staining with DiD, a fluorescent dye that labels cell membranes[26] showed no evidence that the released SG-like particles were membrane-enclosed (Extended Data Fig. 5c), suggesting that CTS is unlikely to occur through classical membrane-bound vesicles.

To further identify the secretory route, we performed a targeted pharmacological screen using inhibitors of conventional ER-Golgi secretion (brefeldin A) and of several UPS pathways, including bufalin (Na^+/K^+-ATPase-associated type I UPS), glibenclamide (type II UPS) and 3-methyladenine (3-MA; type III UPS)[16,27-31]. Among these treatments, only 3-MA substantially reduced SG release (Extended Data Fig. 5d,e), indicating the involvement of type III UPS pathway. We then generated *TMED10*-deficient HK-2 cells to genetically validates this finding, as TMED10 is a key regulator of type III UPS[31,32]. *TMED10* deficiency markedly attenuated stress-induced secretion of G3BP1 and TIA-1, and this defect was fully rescued by *TMED10* re-expression (Fig. 3a,b). We also generated *TMED10* knockout and rescue lines in mCherry-G3BP1-expressing cells (Extended Data Fig. 5f). Consistently, Transwell co-culture assays showed that *TMED10* deficiency in donor cells significantly reduced SG transfer to recipient cells (Fig. 3c–e).

Next, we tested the effect of TMED10-dependent release on ISR propagation. While TMED10 deficiency did not impair cell-autonomous SG formation (Extended Data Fig. 5g) or ISR activation (Extended Data Fig. 5h,i) in response to arsenite or poly(I:C), it dampened the ISR activation in wild-type recipient cells in the lower chamber. Consistently, *TMED10* re-expression in donor cells restored ISR activation in recipients (Fig. 3f–i and Extended Data Fig. 5j). Together, these data indicate that TMED10-dependent type III UPS is required for the release of SGs to propagate ISR activation.

Macropinocytosis mediates SG uptake and CTS-driven ISR activation

We then sought to investigate the entry route by which extracellular SG droplets are internalized by recipient cells. Recipient cells were treated with inhibitors targeting macropinocytosis (amiloride, AM), clathrin-mediated endocytosis (chlorpromazine, CP), or

lipid raft–mediated endocytosis (methyl-β-cyclodextrin, M-β-CD)[33]. As a positive control, cells were also incubated at 4 °C, a condition that broadly inhibits endocytic uptake[34]. Among these perturbations, only AM and 4 °C effectively blocked uptake of mEGFP-G3BP1 droplets (Extended Data Fig. 6a–d), suggesting macropinocytosis as the major entry route. In line with these results, genetic ablation of any of core regulators of macropinocytosis, *CTBP1*, *RAC1* or *ANKFY1*, substantially impaired the internalization of mEGFP-G3BP1:poly(A) condensates (Fig. 4a–d and Extended Data Fig. 6e). Re-expression of the respective genes significantly rescued the defect (Fig. 4e,f and Extended Data Fig. 6f,g).

We further assessed whether macropinocytosis is required for CTS-dependent ISR propagation. Deficiency of *CTBP1*, *RAC1* or *ANKFY1* did not impair cell-autonomous ISR activation in response to arsenite or poly(I:C) (Extended Data Fig. 7a–f), but abolished ISR activation induced by mEGFP-G3BP1:poly(A) droplets (Fig. 4g,h and Extended Data Fig. 8a–d). Consistently, in Transwell co-culture systems, stressed donors in upper chamber failed to elicit ISR signaling in recipient cells lacking *CTBP1* (Fig. 4i–m), *RAC1* (Extended Data Fig. 8e–h) or *ANKFY1* (Extended Data Fig. 8i–l). This indicates that macropinocytosis is required both for uptake of SG droplets and the intercellular ISR propagation. Together, these findings delineate a complete intercellular circuit wherein stress-induced SGs are released *via* TMED10-dependent unconventional secretion and internalized through macropinocytosis, thereby enabling CTS-driven ISR propagation (Fig. 4n).

Inhibiting CTS mitigates renal IRI by dampening the ISR in tissues

To evaluate the pathophysiological relevance of the CTS *in vivo*, we employed a murine model of renal IRI, a condition in which dysregulated ISR activation contributes to tissue damage[3]. We first confirmed SG formation in IRI kidney tissue by immunofluorescence detection of G3BP1-positive puncta (Fig. 5a). Renal injury was assessed by the measurement of serum biomarkers (urea, creatinine and uric acid) (Extended Data Fig. 9a), histopathology (hematoxylin and eosin staining) (Extended Data Fig. 9b) and transcriptomic analysis of ISR-associated signatures (Extended Data Fig. 9c).

To test whether the disruption of CTS could mitigate tissue injury in renal IRI, we

generated kidney-specific conditional knockout mice lacking either *G3bp1* or *Ctbp1*. Following renal IRI, both *G3bp1*- and *Ctbp1*-conditional knockout mice exhibited significantly reduced kidney injury, as evidenced by improved renal function with reduced serum urea, creatinine and uric acid levels (Fig. 5b), less severe histopathology and lower injury scores (Fig. 5c,d) and attenuated ISR activation in kidney tissue, as assessed by qPCR of ISR-associated genes (Fig. 5e). These findings collectively indicate the involvement of SG assembly and macropinocytosis-dependent uptake in tissue injury during renal IRI.

We next examined whether pharmacological inhibition of SG release or uptake could phenocopy these genetic perturbations. Pretreatment with 3-MA reduced renal injury and improved renal function following IRI (Fig. 5f–h), accompanied by diminished ISR-associated transcriptional responses (Fig. 5i). Similar protection was observed in amiloride-treated mice, which also exhibited reduced renal injury and attenuated ISR activation (Extended Data Fig. 9d–g). The consistency between the genetical and pharmacological interventions further supports involvement of the CTS pathway in IRI progression.

Together, our findings present a model wherein renal IRI induces CTS for the ISR propagation in kidney tissues, highlighting CTS as a potentially actionable therapeutic target in renal IRI and other diseases driven by ISR.

Discussion

While the ISR is traditionally defined as a cell-autonomous program, tissue injury often extends beyond the initially stressed cells. Here we identify cell-to-cell transmission of stress granules (CTS) as an intercellular mechanism that propagates ISR activation. Our identification of CTS redefines SGs from passive intracellular adaptors into active intercellular effectors that broadcast stress across cellular boundaries. This finding suggests a plausible molecular basis for previously observed intercellular stress signaling, such as transmissible ER stress[4,15], illustrating a condensate-mediated mode of ISR propagation.

A central conceptual implication of our study is that ISR initiation and ISR propagation are mechanistically separable. Directly stressed donor cells mounted a robust, cell-

autonomous ISR even when SG assembly was blocked, consistent with evidence that translational repression and SG biogenesis can be uncoupled[10,20]. By contrast, ISR activation in recipient cells depended specifically on the condensed, rather than soluble, state of SG material. This suggests that condensation packages RNAs and proteins into assemblies with high local concentration and multivalency, creating a signaling-competent machinery that dispersed soluble components cannot provide. In this sense, CTS transmits not merely molecular cargo, but a higher-order organization of stress-associated material.

Our data identify a TMED10-linked unconventional secretory pathway and macropinocytosis as key enabling steps for CTS. This transfer route implies that recipient-cell ISR activation is triggered by uptake of pre-assembled SG material rather than by exposure to individual soluble ligands. An interesting observation is that CTS-induced ISR specifically requires PERK and GCN2 in recipient cells, but not PKR or HRI. This raises the question of how internalized SG condensates engage these specific kinases. One possibility is that SGs contain or recruit specific RNA species, such as uncharged tRNAs or amino acid-starvation, which directly activate GCN2[2,35]. Alternatively, the macropinocytic uptake of large condensates may burden the endolysosomal system or disrupt ER homeostasis, thereby engaging PERK through membrane contact sites between internalized SG-containing vesicles and the ER. Furthermore, the high-density, multivalent nature of the condensate may provide a scaffold that clusters PERK and GCN2, promoting their oligomerization and subsequent auto-activation.

Several important questions remain open. First, it has yet to be established whether the extracellular droplet represents an intact SG, a remodeled SG-derived assembly, or a closely associated SG cargo complex. The observation that TMED10-dependent secretion releases core SG components (G3BP1, TIA-1) without membrane enclosure suggests a non-vesicular entity, but its precise ultrastructure requires cryo-electron tomography or other high-resolution approaches. Second, the potential contribution of other stress-transmitting signals *in vivo* requires further investigation. It remains possible that other intercellular signals, such as exosomes, free dsRNA, or reactive oxygen species, coexist with CTS. Under our study conditions, the requirement for donor-cell G3BP1 indicates that SG transmission is necessary

for the observed propagation. Third, different stressors may produce SGs with distinct compositions, potentially leading to variable transmissibility or recipient-kinase specificity. Systematic analysis of SG cargo heterogeneity will be important. Fourth, while our *in vivo* genetic and pharmacological interventions demonstrate that SG assembly and uptake are required for renal IRI pathology, these experiments do not directly visualize or prove that intercellular SG transmission itself occurs *in vivo*. Developing tools for real-time *in vivo* imaging of CTS will be essential to establish its occurrence. In addition, while we focused on renal IRI, the CTS pathway may operate in other diseases where deregulated ISR spreads, such as neurodegeneration or chronic inflammatory conditions[1].

The *in vivo* relevance of this pathological amplification is underscored by the role of CTS in renal IRI, a setting in which localized cellular stress progresses into broader tissue dysfunction[3,36]. Genetic disruption of SG assembly or their uptake, as well as pharmacological inhibition of SG release or macropinocytosis, attenuated renal injury and dampened ISR activation *in vivo*. These findings suggest a therapeutic strategy conceptually distinct from global ISR inhibition. Directly blocking eIF2α phosphorylation or PERK may compromise essential adaptive responses in primary-stressed cells[1,2,37]. By contrast, targeting the CTS pathway, for instance by inhibiting SG secretion or uptake, could preferentially limit the spatial spread of pathological stress signaling while preserving the cell-autonomous ISR in directly injured cells. It is worth mentioning that targeting this pathway presents certain challenges. For example, SGs and their associated machinery also contribute to host defense and stress tolerance in certain contexts[38-41], and currently available pharmacological agents such as 3-MA and amiloride have broad effects. Nonetheless, these challenges do not diminish the therapeutic attractiveness of CTS, rather, they define a clear roadmap for future optimization. Moreover, the dispensability of SGs for cell-autonomous ISR in directly stressed cells suggests that selective inhibition of SG transmission may spare protective stress responses at the initial injury site. Developing selective inhibitors of TMED10-dependent secretion, identifying unique surface features of transmissible SG assemblies, or blocking SG-kinase interactions in recipient cells are all viable strategies. Thus, despite current limitations, CTS represents a therapeutically actionable axis in ISR-

associated diseases, and the path toward specific pathway modulation is clearly delineated.

In summary, our work identifies a condensate-based intercellular communication pathway that propagates ISR activation across cell populations. By delineating the molecular steps of SG release, uptake, and downstream kinase engagement, it provides a framework for understanding how locally initiated stress scales to tissue-level pathology and opens new avenues for therapeutic intervention in ISR-associated diseases.

References

1 Costa-Mattioli, M. & Walter, P. The integrated stress response: From mechanism to disease. *Science* **368** (2020). https://doi.org/10.1126/science.aat5314

2 Pakos-Zebrucka, K. *et al.* The integrated stress response. *EMBO Rep* **17**, 1374–1395 (2016). https://doi.org/10.15252/embr.201642195

3 Zhang, G., Wang, X., Rothermel, B. A., Lavandero, S. & Wang, Z. V. The integrated stress response in ischemic diseases. *Cell Death Differ* **29**, 750–757 (2022). https://doi.org/10.1038/s41418-021-00889-7

4 Taylor, R. C., Berendzen, K. M. & Dillin, A. Systemic stress signalling: understanding the cell non-autonomous control of proteostasis. *Nat Rev Mol Cell Biol* **15**, 211–217 (2014). https://doi.org/10.1038/nrm3752

5 Harding, H. P. *et al.* Regulated translation initiation controls stress-induced gene expression in mammalian cells. *Mol Cell* **6**, 1099–1108 (2000). https://doi.org/10.1016/s1097-2765(00)00108-8

6 Klein, P. *et al.* Temporal control of the integrated stress response by a stochastic molecular switch. *Sci Adv* **8**, eabk2022 (2022). https://doi.org/10.1126/sciadv.abk2022

7 Protter, D. S. W. & Parker, R. Principles and Properties of Stress Granules. *Trends Cell Biol* **26**, 668–679 (2016). https://doi.org/10.1016/j.tcb.2016.05.004

8 Banani, S. F., Lee, H. O., Hyman, A. A. & Rosen, M. K. Biomolecular condensates: organizers of cellular biochemistry. *Nat Rev Mol Cell Biol* **18**, 285–298 (2017). https://doi.org/10.1038/nrm.2017.7

9 Anderson, P. & Kedersha, N. Stress granules: the Tao of RNA triage. *Trends Biochem Sci* **33**, 141–150 (2008). https://doi.org/10.1016/j.tibs.2007.12.003

10 Chen, C. W. *et al.* Plasticity of the mammalian integrated stress response. *Nature* **641**, 1319–1328 (2025). https://doi.org/10.1038/s41586-025-08794-6

11 Aulas, A. *et al.* G3BP1 promotes stress-induced RNA granule interactions to preserve polyadenylated mRNA. *J Cell Biol* **209**, 73–84 (2015). https://doi.org/10.1083/jcb.201408092

12 Kedersha, N. *et al.* G3BP-Caprin1-USP10 complexes mediate stress granule condensation and associate with 40S subunits. *J Cell Biol* **212**, 845–860 (2016). https://doi.org/10.1083/jcb.201508028

13 Wolozin, B. & Ivanov, P. Stress granules and neurodegeneration. *Nat Rev Neurosci* **20**, 649–666 (2019). https://doi.org/10.1038/s41583-019-0222-5
14 Mateju, D. *et al.* Single-Molecule Imaging Reveals Translation of mRNAs Localized to Stress Granules. *Cell* **183**, 1801–1812.e1813 (2020). https://doi.org/10.1016/j.cell.2020.11.010
15 Mahadevan, N. R. *et al.* Transmission of endoplasmic reticulum stress and pro-inflammation from tumor cells to myeloid cells. *Proc Natl Acad Sci U S A* **108**, 6561–6566 (2011). https://doi.org/10.1073/pnas.1008942108
16 Rabouille, C. Pathways of Unconventional Protein Secretion. *Trends Cell Biol* **27**, 230–240 (2017). https://doi.org/10.1016/j.tcb.2016.11.007
17 Sparn, C., Meyer, A., Saleppico, R. & Nickel, W. Unconventional secretion mediated by direct protein self-translocation across the plasma membranes of mammalian cells. *Trends Biochem Sci* **47**, 699–709 (2022). https://doi.org/10.1016/j.tibs.2022.04.001
18 Doherty, G. J. & McMahon, H. T. Mechanisms of endocytosis. *Annu Rev Biochem* **78**, 857–902 (2009). https://doi.org/10.1146/annurev.biochem.78.081307.110540
19 Swanson, J. A. Shaping cups into phagosomes and macropinosomes. *Nat Rev Mol Cell Biol* **9**, 639–649 (2008). https://doi.org/10.1038/nrm2447
20 Wu, Y. *et al.* Translation landscape of stress granules. *Sci Adv* **11**, eady6859 (2025). https://doi.org/10.1126/sciadv.ady6859
21 Guillén-Boixet, J. *et al.* RNA-Induced Conformational Switching and Clustering of G3BP Drive Stress Granule Assembly by Condensation. *Cell* **181**, 346–361.e317 (2020). https://doi.org/10.1016/j.cell.2020.03.049
22 Yang, P. *et al.* G3BP1 Is a Tunable Switch that Triggers Phase Separation to Assemble Stress Granules. *Cell* **181**, 325–345.e328 (2020). https://doi.org/10.1016/j.cell.2020.03.046
23 Sanders, D. W. *et al.* Competing Protein-RNA Interaction Networks Control Multiphase Intracellular Organization. *Cell* **181**, 306–324.e328 (2020). https://doi.org/10.1016/j.cell.2020.03.050
24 McEwen, E. *et al.* Heme-regulated inhibitor kinase-mediated phosphorylation of eukaryotic translation initiation factor 2 inhibits translation, induces stress granule formation, and mediates survival upon arsenite exposure. *J Biol Chem* **280**, 16925–16933 (2005). https://doi.org/10.1074/jbc.M412882200
25 Sharma, N. R., Majerciak, V., Kruhlak, M. J. & Zheng, Z. M. KSHV inhibits stress granule formation by viral ORF57 blocking PKR activation. *PLoS Pathog* **13**, e1006677 (2017). https://doi.org/10.1371/journal.ppat.1006677
26 Gan, W. B., Grutzendler, J., Wong, W. T., Wong, R. O. & Lichtman, J. W. Multicolor "DiOlistic" labeling of the nervous system using lipophilic dye combinations. *Neuron* **27**, 219–225 (2000). https://doi.org/10.1016/s0896-6273(00)00031-3
27 Klausner, R. D., Donaldson, J. G. & Lippincott-Schwartz, J. Brefeldin A: insights into the control of membrane traffic and organelle structure. *J Cell Biol* **116**, 1071–1080 (1992). https://doi.org/10.1083/jcb.116.5.1071
28 Numazawa, S., Shinoki, M. A., Ito, H., Yoshida, T. & Kuroiwa, Y. Involvement of Na+,K(+)-ATPase inhibition in K562 cell differentiation induced by bufalin. *J Cell Physiol* **160**, 113–120 (1994). https://doi.org/10.1002/jcp.1041600114
29 Hamon, Y. *et al.* Interleukin-1beta secretion is impaired by inhibitors of the Atp binding cassette transporter, ABC1. *Blood* **90**, 2911–2915 (1997).

30 Dupont, N. *et al.* Autophagy-based unconventional secretory pathway for extracellular delivery of IL-1β. *Embo j* **30**, 4701–4711 (2011). https://doi.org/10.1038/emboj.2011.398
31 Zhang, M. *et al.* A Translocation Pathway for Vesicle-Mediated Unconventional Protein Secretion. *Cell* **181**, 637–652.e615 (2020). https://doi.org/10.1016/j.cell.2020.03.031
32 Sun, Y. *et al.* A dual role of ERGIC-localized Rabs in TMED10-mediated unconventional protein secretion. *Nat Cell Biol* **26**, 1077–1092 (2024). https://doi.org/10.1038/s41556-024-01445-4
33 Banushi, B., Joseph, S. R., Lum, B., Lee, J. J. & Simpson, F. Endocytosis in cancer and cancer therapy. *Nat Rev Cancer* **23**, 450–473 (2023). https://doi.org/10.1038/s41568-023-00574-6
34 Teo, S. L. Y. *et al.* Unravelling cytosolic delivery of cell penetrating peptides with a quantitative endosomal escape assay. *Nat Commun* **12**, 3721 (2021). https://doi.org/10.1038/s41467-021-23997-x
35 Dong, J., Qiu, H., Garcia-Barrio, M., Anderson, J. & Hinnebusch, A. G. Uncharged tRNA activates GCN2 by displacing the protein kinase moiety from a bipartite tRNA-binding domain. *Mol Cell* **6**, 269–279 (2000). https://doi.org/10.1016/s1097-2765(00)00028-9
36 Sharfuddin, A. A. & Molitoris, B. A. Pathophysiology of ischemic acute kidney injury. *Nat Rev Nephrol* **7**, 189–200 (2011). https://doi.org/10.1038/nrneph.2011.16
37 Hetz, C. & Saxena, S. ER stress and the unfolded protein response in neurodegeneration. *Nat Rev Neurol* **13**, 477–491 (2017). https://doi.org/10.1038/nrneurol.2017.99
38 Arimoto, K., Fukuda, H., Imajoh-Ohmi, S., Saito, H. & Takekawa, M. Formation of stress granules inhibits apoptosis by suppressing stress-responsive MAPK pathways. *Nat Cell Biol* **10**, 1324–1332 (2008). https://doi.org/10.1038/ncb1791
39 Thedieck, K. *et al.* Inhibition of mTORC1 by astrin and stress granules prevents apoptosis in cancer cells. *Cell* **154**, 859–874 (2013). https://doi.org/10.1016/j.cell.2013.07.031
40 Liu, Z. S. *et al.* G3BP1 promotes DNA binding and activation of cGAS. *Nat Immunol* **20**, 18–28 (2019). https://doi.org/10.1038/s41590-018-0262-4
41 Zhao, M. *et al.* The stress granule protein G3BP1 promotes pre-condensation of cGAS to allow rapid responses to DNA. *EMBO Rep* **23**, e53166 (2022). https://doi.org/10.15252/embr.202153166

Methods

Antibodies and reagents

Anti-G3BP1 (13057-2-AP), anti-GADD34 (10449-1-AP), anti-TMED10 (15199-1-AP), anti-α-tubulin (66031-1-Ig), anti-GAPDH (60004-1-Ig) and anti-β-actin (66009-1-Ig) were purchased from Proteintech. Anti-CTBP1 (8684S), anti-phospho-eIF2α (Ser51) (3398S), anti-eIF2α (5324S), anti-ATF4 (11815S) and anti-CHOP (2895S) were from Cell Signaling Technology. Anti-TIA-1 (sc-166247), anti-GCN2 (sc-374609) and anti-ANKFY1 (sc-393353) were from

Santa Cruz Biotechnology. Anti-RAC1 (05-389) and anti-puromycin (MABE343) were from Merck Millipore. Anti-PERK (ab65142) was from Abcam. Anti-EGFP (MA1-952) and Goat anti-Rabbit IgG AF488, Goat anti-Mouse IgG AF488, Goat anti-Mouse IgG AF647 and Goat anti-Rabbit IgG AF647 were from Invitrogen.

Poly(A) RNA (10108626001) was purchased from Roche. Poly(I:C) (tlrl-picb) was from InvivoGen. Alexa Fluor 647-conjugated wheat germ agglutinin (WGA-647, MP6335) and WGA-488 (MP6325) were from Shanghai Maokang Biotechnology. Sodium arsenite (S7400) was from Sigma-Aldrich. ActinRed™ 555 ReadyProbes™(R37112), Lipofectamine 2000 (11668019) and Lipofectamine™ RNAiMAX (13778150) were from Thermo Fisher Scientific. Methyl-β-cyclodextrin (M-β-CD; T4072), 2-deoxy-D-glucose (2-DG; T6742), bufalin (T1719), 3-methyladenine (3-MA; T1879), brefeldin A (T6062) and glibenclamide (T1634) were from TargetMol Chemicals. Amiloride (AM; HY-B0285A) and chlorpromazine (CP; HY-12708) were from MedChemExpress. Creatinine (Cr) Colorimetric Assay Kit (E-BC-K188-M), Urea (BUN) Colorimetric Assay Kit (E-BC-K183-M) and Uric Acid (UA) Colorimetric Assay Kit (E-BC-K016-M) were from Elabscience.

Cell lines and culture conditions

H1299 (CRL-5803), AC16 (CRL-3568) and HeLa cells (CCL-2) were obtained from ATCC. HK-2 (CL-0109) and HEK293T cells (CL-0005) were obtained from Wuhan Procell. Cells were cultured in Minimum Essential Medium (MEM, HK-2), RPMI-1640 medium (H1299), DMEM/F12 medium (AC16) or DMEM (HeLa, HEK293T) supplemented with 10% fetal bovine serum (FBS), 2 mM L-glutamine, 1 mM sodium pyruvate, 100 U mL^{-1} penicillin and 100 μg mL^{-1} streptomycin at 37 °C in 5% CO_2. Cell lines were routinely tested and confirmed to be free of mycoplasma contamination.

Generation of gene-deficient and rescued cell lines

Gene knockout HK-2 cell lines (*G3BP1*, *CTBP1*, *RAC1*, *ANKFY1*, *TMED10, GCN2 and PERK*) were generated using the lentiCRISPRv2 (Blasticidin) system. Single-guide RNAs (sgRNAs) were designed using CHOPCHOP (https://chopchop.cbu.uib.no/). Lentiviral

particles were produced in HEK293T cells by co-transfecting lentiCRISPRv2-sgRNA with psPAX2 and pVSVG packaging plasmids using MaxiCaP (MACGENE Biotechnology, CTK001). Target cells were transduced with viral supernatant and selected with blasticidin (4 μg mL^{-1}).

For rescue experiments, the corresponding cDNAs were cloned into pLVX-neomycin vector and introduced into knockout cells by lentiviral transduction, followed by neomycin selection (500 μg mL^{-1}). sgRNA and primer sequences are provided in Supplementary Table 1. Knockout and rescue efficiency were validated by immunoblotting.

Plasmid construction

Full-length human cDNAs encoding *G3BP1*, *CTBP1*, *RAC1*, *ANKFY1* and *TMED10* were amplified and subcloned into pLVX-neomycin vector for mammalian expression. Fluorescent SGs reporters (mCherry-G3BP1 and G3BP1-mEGFP) were also cloned into pLVX-Puro or pLVX-neomycin. For bacterial expression, mEGFP-G3BP1 and TAT-mEGFP-G3BP1 were inserted into pET-28a(+) to generate N-terminal 6×His-tagged fusion proteins. All constructs were verified by Sanger sequencing.

Mouse models

All animal procedures were approved by the Institutional Animal Care and Use Committee (IACUC) of Nanhu Laboratory (Ethics Approval Nos. IACUC-NHLAC-2025-018 and IACUC-NHLAC-2025-010). *G3bp1*$^{fl/fl}$, *Ctbp1*$^{fl/fl}$ and *Ggt1*-Cre mice were generated by Cyagen Biosciences. Kidney-specific knockout mice were generated by crossing *Ggt1*-Cre mice with the corresponding floxed strains. Mice were maintained under specific-pathogen-free conditions with ad libitum access to food and water.

Blue light-induced SG formation

Live-cell imaging was performed using a spinning disk confocal microscope (Dragonfly 200, Andor) equipped with a 40×/1.3 NA oil immersion objective. Cells (Cry2-mCherry-G3BP1-AC16 and G3BP1-mEGFP-AC16) were seeded 24 h before imaging onto 35 mm glass-bottom dishes with four wells (D35C4-20-1.5-N, Cellvis). Before imaging,

the culture medium was replaced with Fluoro-Brite DMEM (A1896701, Thermo Fisher) supplemented with 10% fetal bovine serum (FBS). During imaging, cells were maintained at 37 °C in an environmental control chamber, and Definite Focus was used to prevent focal drift. Before photoactivation, an initial image was acquired using 20% 488 nm laser (50 ms exposure) and 30% 546 nm laser (100 ms exposure) to record the baseline state. Subsequently, a 1 s pulse of 100% 488 nm laser was applied for 5 min to activate the cells, followed by a 3 min pause. This 5 min activation – 3 min pause cycle was repeated once (total activation time 10 min) to induce stress granule formation. After activation, cells were imaged every 6 min using the same exposure settings (20% 488 nm, 50 ms; 30% 546 nm, 100 ms). Image analysis and 3D reconstruction were performed using Imaris software (Bitplane).

Recombinant protein purification

pET-28a(+) constructs encoding mEGFP-G3BP1 or TAT-mEGFP-G3BP1 were transformed into *E. coli* BL21 (DE3). Cultures were grown in LB medium at 37 °C to OD_{600} = 0.8-1.0, and protein expression was induced with 0.5 mM IPTG at 18 °C for 18-20 h. Cells were harvested by centrifugation and lysed in lysis buffer (50 mM NaH_2PO_4, 1.5 M NaCl, pH=7.4) supplemented with protease inhibitors (P1030, Beyotime Biotechnology; SH404-01, Beijing Biomed Gene technology). Recombinant proteins were purified under native conditions using Ni-NTA agarose beads (Nickel-NTA Agarose Beads 6FF, G106, Genstar) according to the manufacturer's protocol. Eluted proteins were buffer-exchanged into phase separation buffer (400 mM NaCl, 50 mM HEPES, 1 mM DTT, pH=7.4), filter-sterilized (0.22 μm), aliquoted and stored at -80 °C.

Immunofluorescence staining

Cells were seeded on glass coverslips (72196-12, Electron Microscopy Sciences) in 24-well plates and allowed to adhere overnight. Following treatment, cells were fixed in 4% paraformaldehyde for 15 min at room temperature, permeabilized with 0.1% Triton X-100 in PBS, and blocked in 5% bovine serum albumin (BSA) in PBS for 1 h. Primary antibodies were incubated overnight at 4 °C, followed by fluorophore-conjugated secondary antibodies for 1 h at room temperature. Nuclei were counterstained with Hoechst 33342 (H3570, Thermo

Fisher Scientific.). Coverslips were mounted using antifade mounting medium and imaged on a Zeiss LSM 900 confocal microscope. Image acquisition settings were kept constant within experiments.

RNA isolation and quantitative PCR

Total RNA was extracted using TRIGene Reagent (P118-05, Genstar) following the manufacturer's instructions. RNA concentration and purity were assessed by NanoDrop. cDNA was synthesized from 500 ng total RNA using Evo M-MLV RT Kit (AG11728, Accurate Biotechnology). qPCR was performed using Taq Pro Universal SYBR qPCR Master Mix (Q712-02, Vazyme) on a StepOnePlus Real-Time PCR System (Applied Biosystems). Relative expression was calculated using the $\Delta\Delta C_T$ method, normalized to GAPDH. Primer sequences are listed in Supplementary Table 1.

***In vitro* phase separation assay**

Purified mEGFP-G3BP1 protein was diluted to 50 μM in G3BP1 reaction buffer (GRB: 50 mM HEPES, 50 mM NaCl, 1 mM DTT, pH=7.4). Poly(A) was added to a final concentration of 100 ng μL^{-1} to initiate condensate formation. Droplet formation was monitored at the indicated time points using a Thunder imaging system or a Zeiss LSM 900 confocal microscope with a 63× oil-immersion objective.

Droplet uptake assay

HK-2 cells were plated in a 24-well plate and cultured overnight. mEGFP-G3BP1-poly(A) condensates were prepared as described above and added directly to culture media at 10 μL. Cells were incubated for 6 h for flow cytometry-based uptake quantification, or for 36–48 h for ISR activation analyses, and then processed for downstream assays.

Renal ischaemia–reperfusion injury model

Mice were pretreated once daily for 7 consecutive days before surgery. Amiloride (AM; 10 mg kg^{-1}) was administered intraperitoneally, and 3-methyladenine (3-MA; 15 mg kg^{-1}) was administered by intragastric gavage. Renal IRI was induced under general anaesthesia (50 mg kg^{-1}). Following a dorsal approach, both renal pedicles were exposed and occluded using

non-traumatic vascular clips for 30 min to induce ischemia. Clips were then removed to initiate reperfusion. Sham-operated mice underwent identical procedures without vascular clamping. Kidney tissue and serum were collected at 6 h and 24 h after reperfusion for histological and biochemical analyses.

Serum biochemistry (urea, creatinine and uric acid)

Blood was collected from the orbital venous plexus of anaesthetised mice subjected to I/R or sham surgery. Samples were allowed to clot at room temperature for 30 min and centrifuged at 3,000 × g for 15 min at 4 °C to isolate serum. Serum was aliquoted and stored at -80 °C. Serum urea, creatinine and uric acid were quantified using commercial assay kits (E-BC-K183-M, E-BC-K188-M and E-BC-K016-M; Elabscience) according to the manufacturers' instructions. Absorbance was measured using a microplate reader (SpectraMax i3x), and concentrations were calculated using standard curves supplied with each kit.

Transwell assay

Donor cells were seeded in the upper inserts and recipient cells were seeded in the lower wells of a 24-well transwell plate (3421, Corning Incorporated). After overnight equilibration, donor cells were selectively stimulated by transferring the upper inserts to fresh wells containing medium supplemented with the indicated stimuli (poly(I:C) or arsenite) in the absence of recipient cells. Donors were treated for 5 h (poly(I:C)) or 2 h (arsenite), washed three times with PBS, and then returned to the wells containing pre-plated recipient cells to initiate co-culture. After 36–48 h, recipient cells were harvested and ISR activation was analyzed by immunoblotting.

For puromycin incorporation assays, recipient cells were pulsed with puromycin (4 μg mL^{-1}) for 15 min immediately before collection. Cells were lysed, and newly synthesized polypeptides were detected by immunoblotting using anti-puromycin antibody.

RNA-seq analysis

Total RNA was extracted from cultured cells and subjected to bulk RNA sequencing. Raw reads were quality-checked using FastQC and trimmed with Trimmomatic to remove adaptor

sequences and low-quality bases. Clean reads were aligned to the human reference genome (GRCh38/hg38) using HISAT2, and gene-level counts were generated with featureCounts.

Differential expression analysis was performed in R (v4.4.0) using DESeq2 after filtering lowly expressed genes and normalizing count data. Differentially expressed genes were identified using the following criteria: |log2 fold change| > 0.5 and $P < 0.05$. Gene Ontology enrichment analysis was conducted using clusterProfiler (v4.10.1), with false discovery rate (FDR) < 0.05 considered statistically significant.

Statistical analysis

Statistical analyses were performed using GraphPad Prism 9.4. Data are presented as mean ± s.d.. For comparisons between two groups, two-tailed unpaired Student's *t*-tests were used. $P < 0.05$ was considered statistically significant.

Data availability

All data supporting the findings of this study are included in the Article and its Supplementary Information.

Acknowledgements

This work was supported by the National Natural Science Foundation of China (No. 82130052 to T.L., No. 82341098 to T.Z., and No. 82302491 to M.Z.).

Author contributions

T.L., W.X. and T.Z. supervised the project. T.L., W.X., M.Z. and L.-B.Y. designed the experiments. M.Z. and L.-B.Y. performed the phase separation, immunofluorescence, qPCR and animal assays. M.-Y.F. performed the RNA-seq analysis. C.-X.L. designed the graphic abstract and performed the 3D reconstruction. X.-Q.Z., C.-X.L. and H.-Z.Y. purified the proteins. H.C., L.-B.Y., L.C. and T.X. performed the flow cytometry. K.W., X.X. and S.-N.L. performed the microscopic imaging observation. M.Z., L.-B.Y., Y.Y. and Q.-Y.H. constructed the plasmids and cell lines. A.-L.L., X.-M.Z., K.H. and T.L. analyzed the data. T.L., W.X., M.Z., C.-X.L. and L.-B.Y. wrote and revised the manuscript.

Competing interests

The authors declare no competing interests.

Figures

Fig.1

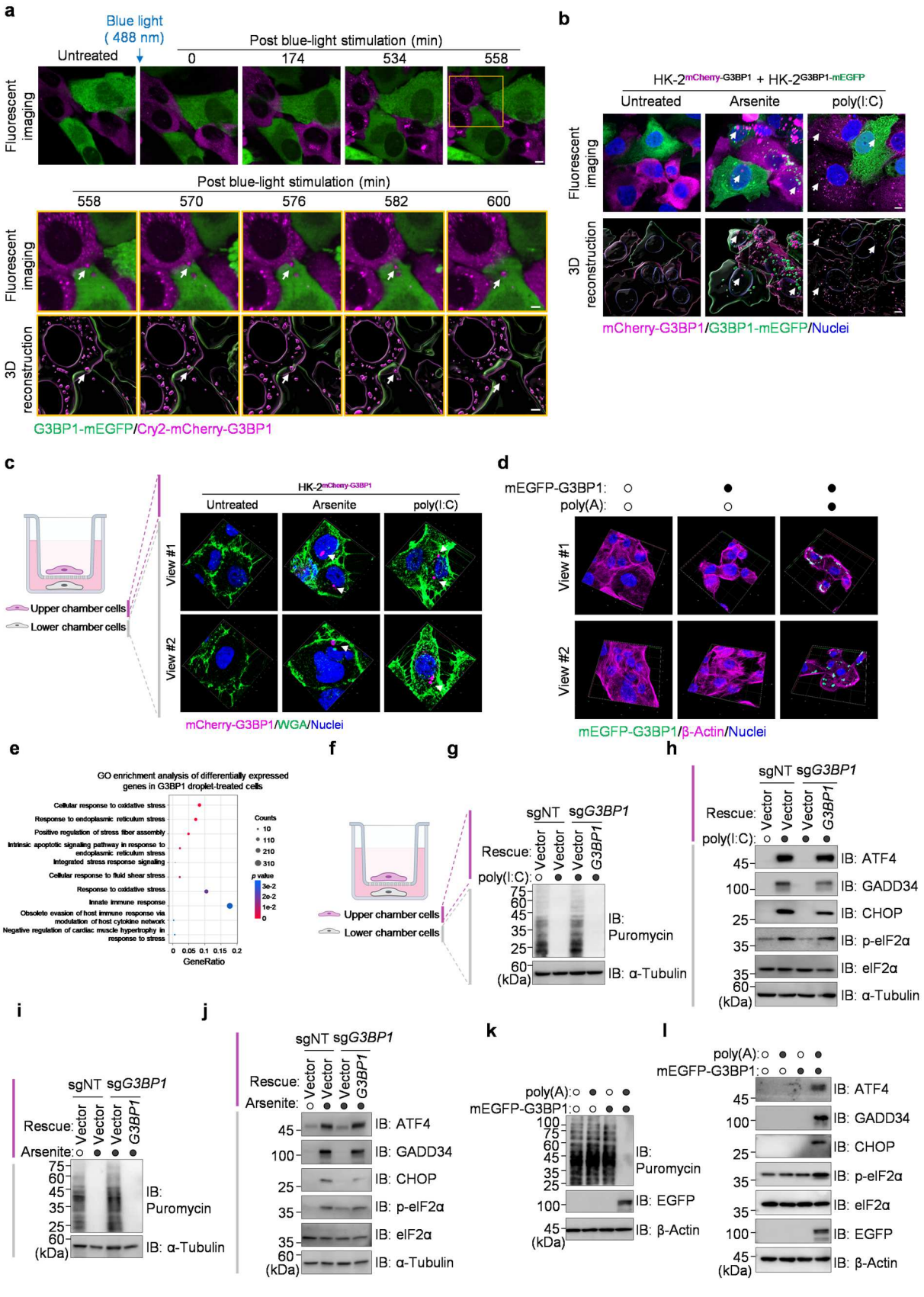


Fig. 1 | Cell-to-cell transmission of stress granules mediates propagation of the ISR. a, Representative images showing the CTS of Opto-SGs in co-cultured AC16 cells expressing fluorescently tagged G3BP1 (Cry2-mCherry-G3BP1 and G3BP1-mEGFP). The cells were treated with blue light, and images were acquired every 6 min. **b**, Representative images of SGs induced by poly(I:C) or arsenite in co-cultured HK-2$^{mCherry\text{-}G3BP1}$ and HK-2$^{G3BP1\text{-}mEGFP}$ cells. The cells were treated with poly(I:C) (1 μg mL^{-1}) for 7 h or arsenite (300 μM) for 3 h. **c**, Transwell assay to assess CTS without direct cell-cell contact. HK-2 donor cells expressing mCherry-G3BP1 were seeded in the upper chamber and stressed with poly(I:C) or arsenite, unlabeled HK-2 recipient cells were cultured in the lower chamber. Left, schematic. Right, representative images showing mCherry-G3BP1-positive SG puncta in recipient cells, plasma membranes were stained with WGA (green). **d**, Uptake of G3BP1 droplets (mEGFP-G3BP1:poly(A)) by HK-2 cells. Droplets were formed *in vitro* (50 μM mEGFP-G3BP1 + 100 ng μL^{-1} poly(A), 10 min) and added to HK-2 cells for 6 h. **e**, RNA-seq and GO analysis were performed on HK-2 cells incubated with G3BP1 droplets as in **d**. **f-j**, Transwell assay using genetically modified HK-2 donor cells (sgNT$^{Vector\ rescue}$, sg*G3BP1*$^{Vector\ rescue}$ or sg*G3BP1*$^{G3BP1\ rescue}$). Donor cells in the upper chamber were stressed with poly(I:C) (1 μg mL^{-1}, 5 h) or arsenite (300 μM, 2 h) in the absence of recipients, then transferred to a new lower chamber containing unstimulated recipient HK-2 cells. Schematic drawing was shown (**f**). Translation in recipients was assessed by puromycin incorporation (**g,i**) and ISR activation was analysed by immunoblotting of recipient lysates (**h,j**) using indicated antibodies. **k**,**l**, HK-2 cells were treated with poly(A), mEGFP-G3BP1 or mEGFP-G3BP1:poly(A) droplets. Translation was assessed by puromycin incorporation (**k**) and ISR activation was analysed by immunoblotting with the indicated antibodies (**l**). Scale bars, 10 (**a,** up) and 5 (a, down; **b**) μm. Nuclei, Hoechst. The images were reconstructed in Imaris (**a**,**b**).

Fig.2

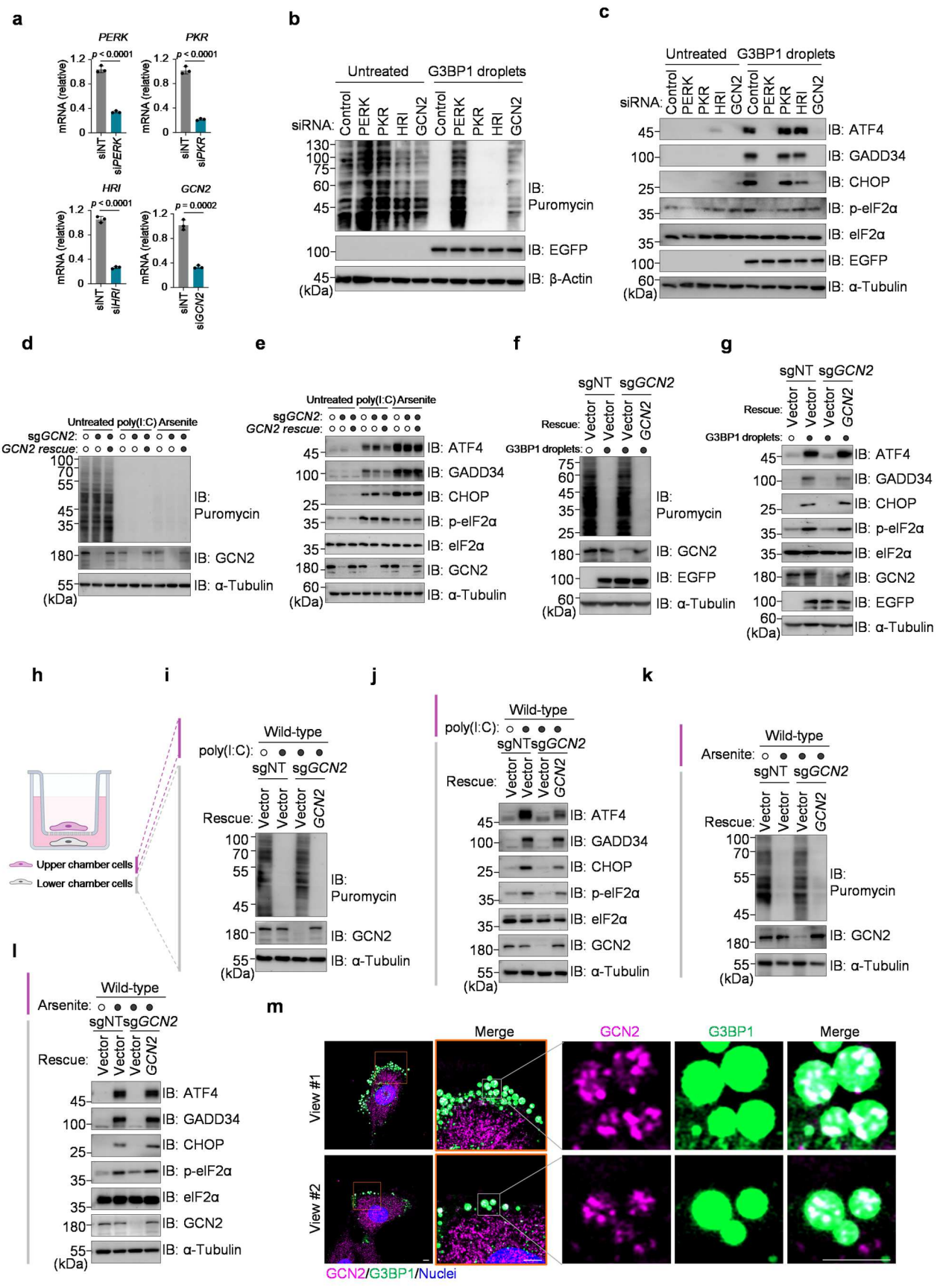

a
PERK
PKR
HRI
GCN2
mRNA (relative)
siNT
siPERK
siPKR
siHRI
siGCN2
b
Untreated
G3BP1 droplets
siRNA:
Control
PERK
PKR
HRI
GCN2
IB: Puromycin
IB: EGFP
IB: β-Actin
(kDa)
c
IB: ATF4
IB: GADD34
IB: CHOP
IB: p-eIF2α
IB: eIF2α
IB: EGFP
IB: α-Tubulin
d
Untreated poly(I:C) Arsenite
sgGCN2:
GCN2 rescue:
IB: Puromycin
IB: GCN2
e
f
sgNT
sgGCN2
Rescue:
Vector
GCN2
G3BP1 droplets:
g
h
Upper chamber cells
Lower chamber cells
i
Wild-type
poly(I:C):
j
k
Arsenite:
l
m
Merge
GCN2
G3BP1
View #1
View #2
GCN2/G3BP1/Nuclei

Fig. 2 | PERK and GCN2 are important for CTS-induced ISR activation. a-c, HK-2 cells with individual knockdown of PERK, PKR, GCN2, or HRI were incubated with G3BP1 droplets for 48 h. Knockdown efficiency was validated by qPCR (**a**). Translation was assessed by puromycin incorporation (**b**) and ISR activation was analyzed by immunoblotting (**c**) using indicated antibodies. **d**,**e**, Genetically modified HK-2 cells (as indicated) were stimulated with poly(I:C) (1 μg mL^{-1}, 7 h) or sodium arsenite (300 μM, 3 h). Translation (**d**) and ISR activation (**e**) were assessed as in **b,c**. **f**,**g**, Genetically modified HK-2 cells ($sgNT^{Vector\ rescue}$, $sgGCN2^{Vector\ rescue}$ or $sgGCN2^{GCN2\ rescue}$) were incubated with G3BP1 droplets. Translation (**f**) and ISR activation (**g**) were assessed as in **b,c**. **h-l**, Transwell assay using WT HK-2 donor cells and genetically modified recipient HK-2 cells (as indicated). Donors were stressed with poly(I:C) (1 μg mL^{-1}, 5 h) or arsenite (300 μM, 2 h) in the absence of recipients, then transferred to a new lower chamber containing unstimulated recipients for co-culture. Schematic drawing was shown (**h**). Translation (**i,k**) and ISR activation (**j,l**) were assessed as in **b,c**. **m**, Representative images showing the colocalization of internalized G3BP1 droplets with endogenous GCN2. HK-2 cells were incubated with droplets for 24 h and stained with an anti-GCN2 antibody. Scale bar, 5 μm. Nuclei, Hoechst. G3BP1 droplets: mEGFP-G3BP1:poly(A). Data are presented as mean ± s.d.. n=3 biological replicates. Statistical significance was determined by two-tailed unpaired Student's *t*-test.

Fig.3

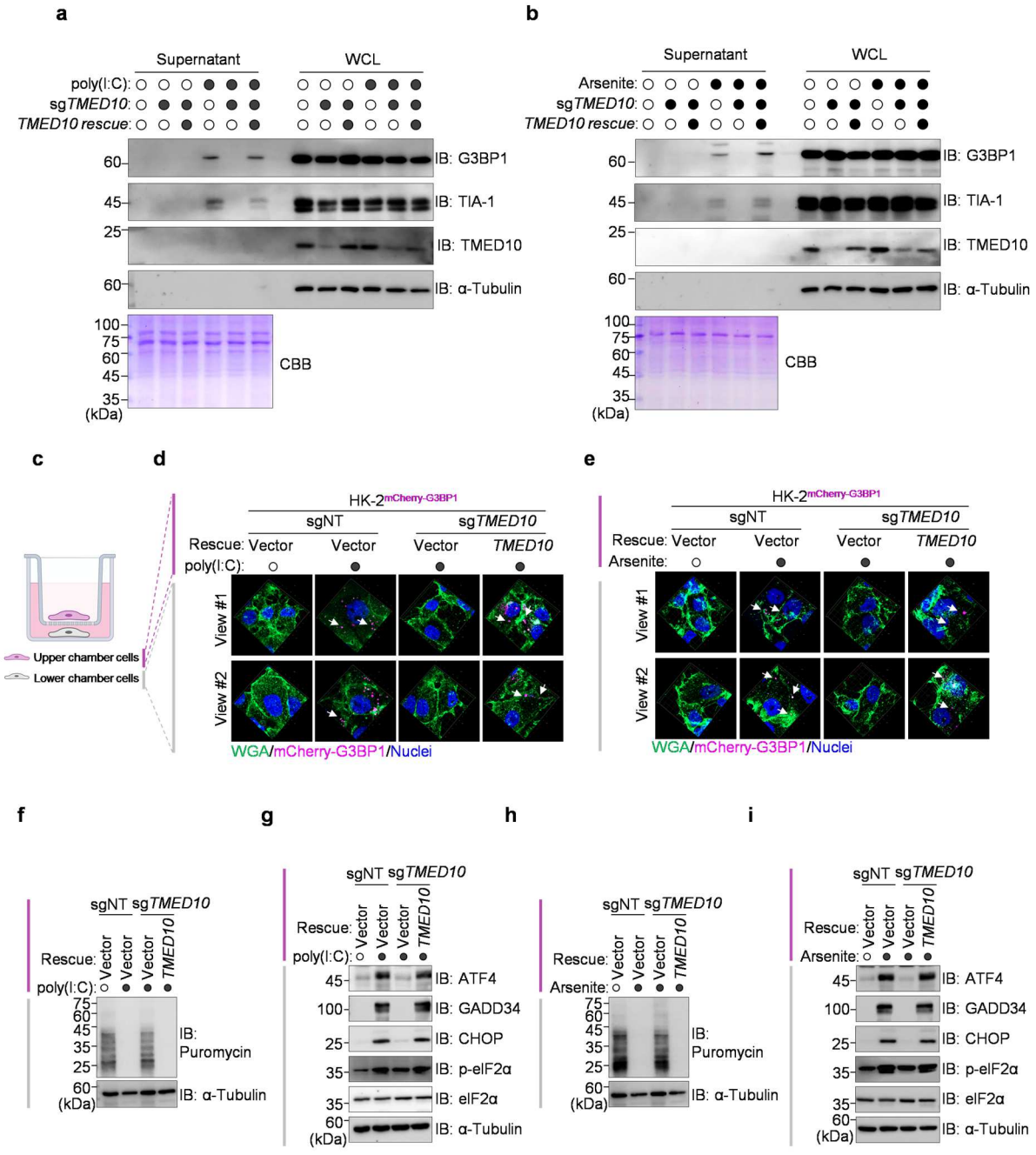

a
Supernatant
WCL
poly(I:C):
sgTMED10:
TMED10 rescue:
IB: G3BP1
IB: TIA-1
IB: TMED10
IB: α-Tubulin
CBB
(kDa)
b
Arsenite:
c
Upper chamber cells
Lower chamber cells
d
HK-2mCherry-G3BP1
sgNT
sgTMED10
Rescue:
Vector
TMED10
View #1
View #2
WGA/mCherry-G3BP1/Nuclei
e
f
IB: Puromycin
g
IB: ATF4
IB: GADD34
IB: CHOP
IB: p-eIF2α
IB: eIF2α
h
i

Fig. 3 | TMED10-dependent type III UPS mediates SG release for ISR propagation. a,**b**, Genetically modified HK-2 donor cells (sgNT$^{\text{Vector rescue}}$, sg*TMED10*$^{\text{Vector rescue}}$ or sg*TMED10*$^{\textit{TMED10}\ \text{rescue}}$) were stimulated with poly(I:C) (1 μg mL^{-1}, 7 h) (**a**) or sodium arsenite (300 μM, 3 h) (**b**). SG release into supernatants was assessed by immunoblotting for G3BP1 and TIA-1; Coomassie blue staining (CBB) of supernatants served as a loading control. **c**-**e**, Transwell assay to monitor CTS from donors to recipients. Donor HK-2 cells expressing mCherry-G3BP1 (genotypes as indicated) were stressed with poly(I:C) (1 μg mL^{-1}, 5 h) (**d**) or arsenite (300 μM, 2 h) (**e**) in the absence of recipients, then transferred to a new lower chamber containing recipient HK-2 cells. Schematic drawing was shown (**c**). Representative images of recipients showing mCherry-G3BP1-positive puncta (magenta). The membranes were stained with WGA (green). **f-i**, Transwell assay to assess ISR propagation. Genetically modified donor HK-2 cells (as in **d,e**) were stressed with poly(I:C) (1 μg mL^{-1}, 5 h) or arsenite (300 μM, 2 h) in the absence of recipients, then transferred to a new lower chamber containing unstimulated recipient HK-2 cells. Translation (**f,h**) and ISR activation (**g,i**) in recipients were assessed by puromycin incorporation and immunoblotting using indicated antibodies, respectively.

Fig.4

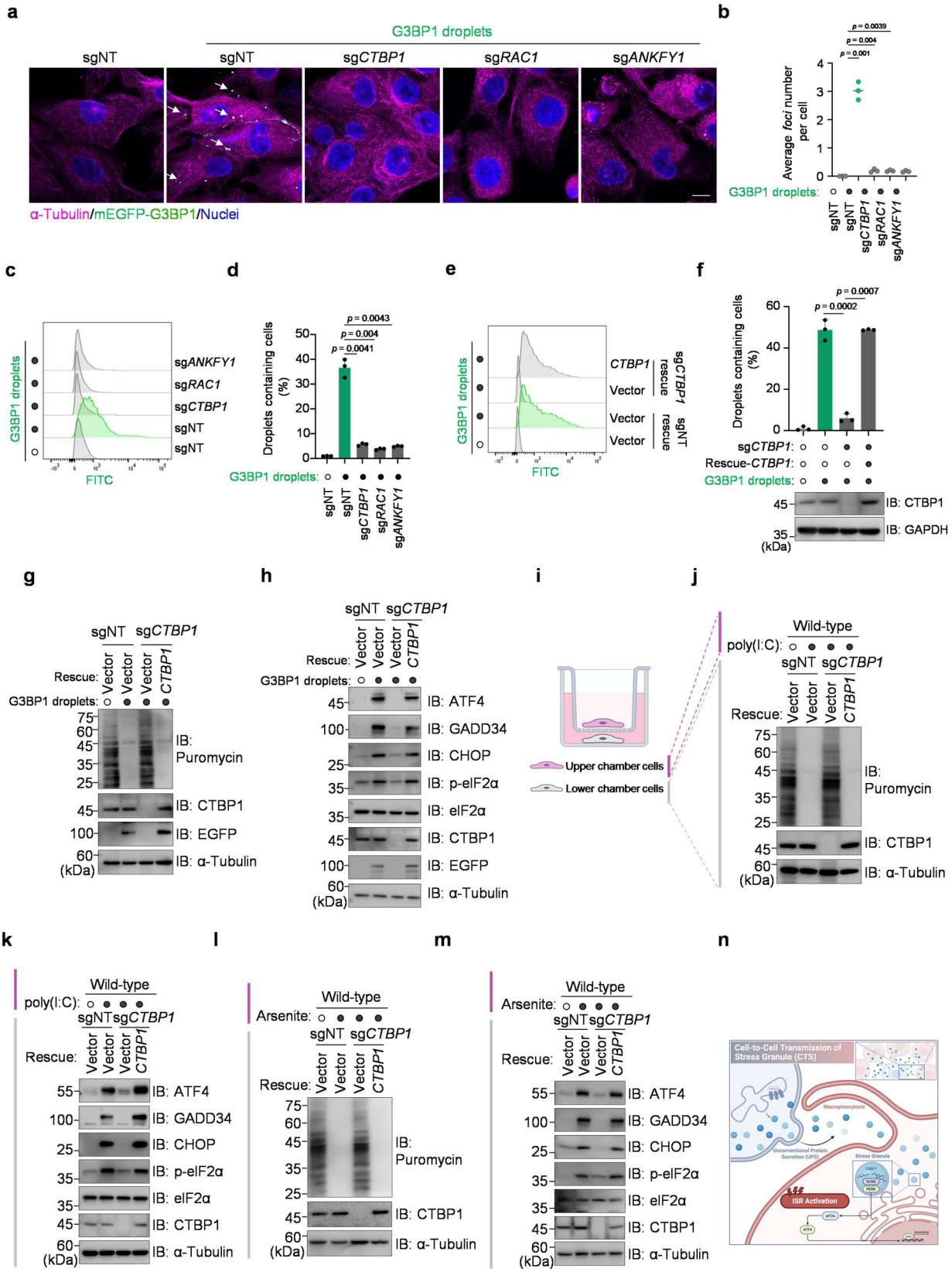

a
G3BP1 droplets
sgNT
sgNT
sgCTBP1
sgRAC1
sgANKFY1
α-Tubulin/mEGFP-G3BP1/Nuclei
b
p = 0.0039
p = 0.004
p = 0.001
Average foci number per cell
G3BP1 droplets:
sgNT
sgNT
sgCTBP1
sgRAC1
sgANKFY1
c
G3BP1 droplets
sgANKFY1
sgRAC1
sgCTBP1
sgNT
sgNT
FITC
d
p = 0.0043
p = 0.004
p = 0.0041
Droplets containing cells (%)
G3BP1 droplets:
sgNT
sgNT
sgCTBP1
sgRAC1
sgANKFY1
e
G3BP1 droplets
CTBP1
Vector
Vector
Vector
sgCTBP1 rescue
sgNT rescue
FITC
f
p = 0.0007
p = 0.0002
Droplets containing cells (%)
sgCTBP1:
Rescue-CTBP1:
G3BP1 droplets:
45
IB: CTBP1
IB: GAPDH
35
(kDa)
g
sgNT
sgCTBP1
Rescue:
Vector
Vector
Vector
CTBP1
G3BP1 droplets:
75
60
45
35
25
IB: Puromycin
45
IB: CTBP1
100
IB: EGFP
60
IB: α-Tubulin
(kDa)
h
sgNT
sgCTBP1
Rescue:
Vector
Vector
Vector
CTBP1
G3BP1 droplets:
45
IB: ATF4
100
IB: GADD34
25
IB: CHOP
35
IB: p-eIF2α
35
IB: eIF2α
45
IB: CTBP1
100
IB: EGFP
60
IB: α-Tubulin
(kDa)
i
Upper chamber cells
Lower chamber cells
j
Wild-type
poly(I:C):
sgNT
sgCTBP1
Rescue:
Vector
Vector
Vector
CTBP1
75
60
45
35
25
IB: Puromycin
45
IB: CTBP1
60
IB: α-Tubulin
(kDa)
k
Wild-type
poly(I:C):
sgNT
sgCTBP1
Rescue:
Vector
Vector
Vector
CTBP1
55
IB: ATF4
100
IB: GADD34
25
IB: CHOP
35
IB: p-eIF2α
35
IB: eIF2α
45
IB: CTBP1
60
IB: α-Tubulin
(kDa)
l
Wild-type
Arsenite:
sgNT
sgCTBP1
Rescue:
Vector
Vector
Vector
CTBP1
75
60
45
35
25
IB: Puromycin
45
IB: CTBP1
60
IB: α-Tubulin
(kDa)
m
Wild-type
Arsenite:
sgNT
sgCTBP1
Rescue:
Vector
Vector
Vector
CTBP1
55
IB: ATF4
100
IB: GADD34
25
IB: CHOP
35
IB: p-eIF2α
35
IB: eIF2α
45
IB: CTBP1
60
IB: α-Tubulin
(kDa)
n
Cell-to-Cell Transmission of Stress Granule (CTS)
Macropinocytosis
Unconventional Protein Secretion (UPS)
Stress Granule
ISR Activation

Fig. 4 | Macropinocytosis mediates SG uptake and CTS-driven ISR activation. a,**b**, HK-2 cells (sgNT, sg*CTBP1*, sg*RAC1*, sg*ANKFY1*) were incubated with G3BP1 droplets for 6 h and analyzed by immunofluorescence to quantify droplet internalization. Representative images were shown (**a**). Average *foci* number per cell was quantified (50 cells per group) (**b**). Scale bar, 10 μm. **c**,**d**, HK-2 cells (as in **a**) were incubated with G3BP1 droplets for 6 h. Uptake was quantified by flow cytometry (**c**) and percentage of droplet-positive cells (**d**). **e**,**f**, Uptake assay performed (as in **c**) using genetically modified HK-2 cells (as indicated). Uptake was quantified by flow cytometry (**e**) and percentage of droplet-positive cells (**f**). **g**,**h**, Genetically modified HK-2 recipient cells (as indicated) were incubated with G3BP1 droplets. Translation (**g**) and ISR activation (**h**) were assessed. **i**-**m**, Transwell assay using WT HK-2 donor cells and genetically modified recipient cells (as indicated). Donors were stressed with poly(I:C) (1 μg mL^{-1}, 5 h) or arsenite (300 μM, 2 h) in the absence of recipients, then transferred to a new lower chamber containing unstimulated recipients. Schematic drawing was shown (**i**). Translation (**j,l**) and ISR activation (**k,m**) in recipients were assessed. **n**, Schematic of CTS. During stress, donor cells secrete SGs *via* TMED10-dependent UPS, which are internalized by recipient cells through macropinocytosis. Internalized SGs associate with GCN2 and PERK, contributing to ISR activation. G3BP1 droplets: mEGFP-G3BP1:poly(A). Data are presented as mean ± s.d.. n= 3 biological replicates. Statistical significance was determined by two-tailed unpaired Student's *t*-test.

Fig.5

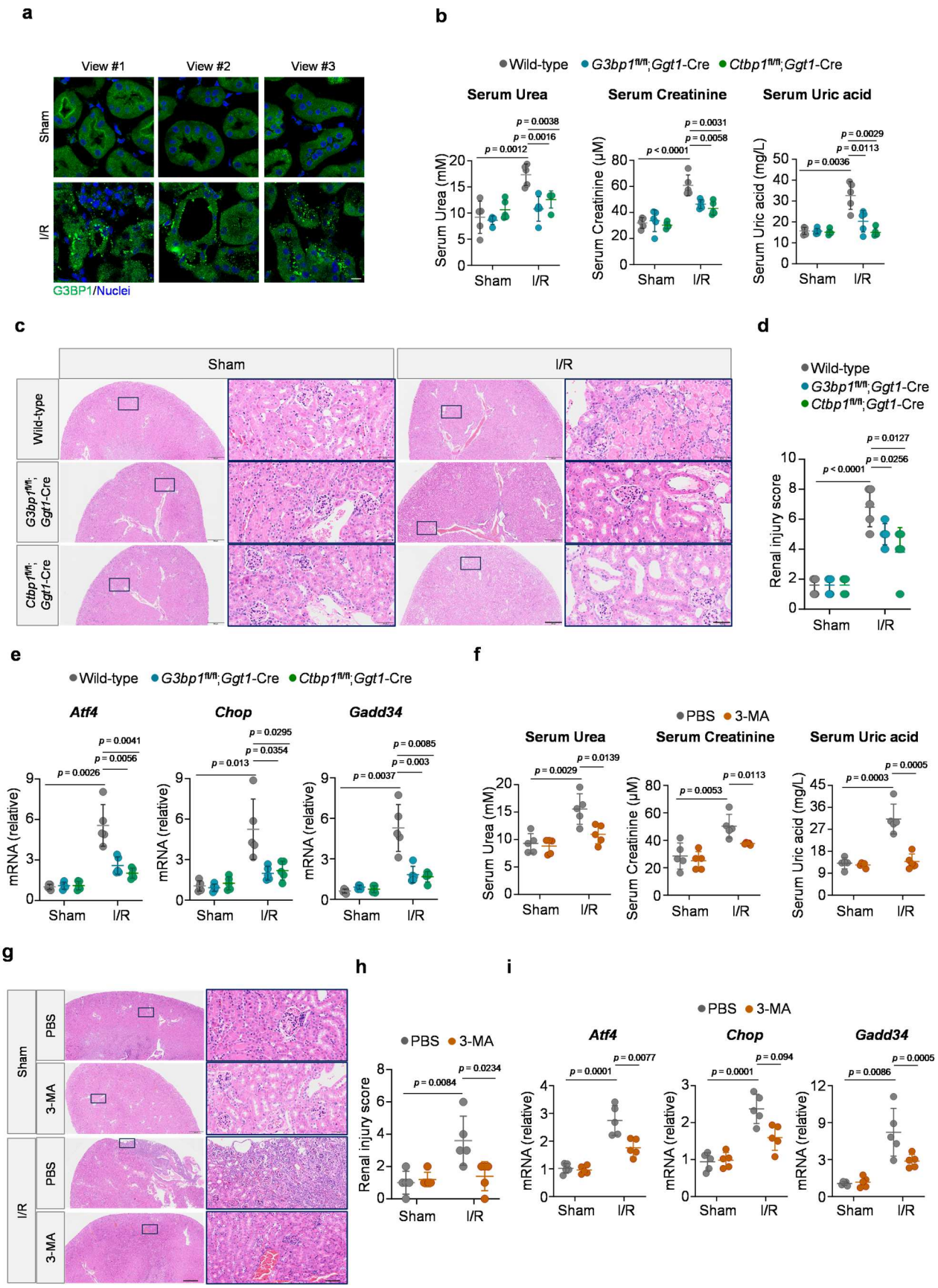

a
View #1
View #2
View #3
Sham
I/R
G3BP1/Nuclei
b
Wild-type
G3bp1fl/fl;Ggt1-Cre
Ctbp1fl/fl;Ggt1-Cre
Serum Urea
Serum Creatinine
Serum Uric acid
Serum Urea (mM)
Serum Creatinine (μM)
Serum Uric acid (mg/L)
Sham
I/R
c
Sham
I/R
Wild-type
G3bp1fl/fl; Ggt1-Cre
Ctbp1fl/fl; Ggt1-Cre
d
Renal injury score
e
Atf4
Chop
Gadd34
mRNA (relative)
f
PBS
3-MA
g
h
i

Fig. 5 | Inhibiting CTS mitigates renal IRI by dampening the ISR. a, Kidney sections from mice subjected to I/R injury were immunostained for G3BP1 (green), representative images were shown. **b**-**e**, Genetic ablation of *G3bp1* or *Ctbp1* in *Ggt1*-Cre mice protects against renal IRI. Serum urea, creatinine and uric acid (**b**), representative H&E-stained kidney sections from sham or I/R kidneys (**c**), renal injury scores (**d**) and qPCR of ISR-related genes (**e**) were shown. **f**-**i**, Pharmacological inhibition with 3-MA attenuates IRI-induced kidney injury. Serum urea, creatinine and uric acid (**f**), representative H&E-stained kidney sections from sham or I/R kidneys (**g**), renal injury scores (**h**) and qPCR of ISR-related genes (**i**) were shown. Scale bars, 10 (**a**), 500 (**c**,**g**, left) or 50 (**c**,**g,** right) μm. Data are presented as mean ± s.d. n = 5 mice. Statistical significance was determined by two-tailed unpaired Student's *t*-test.

Supplementary Files

This is a list of supplementary files associated with this preprint. Click to download.

- Supplementaryvideo3.mp4
- 3SupplementaryTable1.xlsx
- figs7.tif
- figs2.tif
- figs42.tif
- figs3.tif
- figs1.tif
- figs6.tif
- figs8.tif
- fig5.tif
- figs9.tif
- Supplementaryvideo2.avi
- 2Supplementaryinformation.pdf
- Supplementaryvideo1.mp4
- Rawdatagels5M20260513407.pdf
- ExtendedDataFig.620260513407.tif